Available online at www.sciencedirect.com

SCIENCE DIRECT®

Science of the Total Environment 339 (2005) 253–265

Science of the Total Environment
An International Journal for Scientific Research into the Environment and its Relationship with Humankind

www.elsevier.com/locate/scitotenv

Laser ablation ICP-MS profiling and semiquantitative determination of trace element concentrations in desert tortoise shells: documenting the uptake of elemental toxicants

Michael D. Seltzer[a,*], Kristin H. Berry[b]

[a]*Naval Air Warfare Center Weapons Division, Code 4T4230D, 1900 N. Knox Road Stop 6303, China Lake, CA 93555-6106, USA*
[b]*U.S. Geological Survey, Western Ecological Research Center, Box Springs Field Station, 22835 Calle San Juan de Las Lagos, Moreno Valley, CA 92553, United States*

Received 22 March 2004; accepted 22 July 2004

Abstract

The outer keratin layer (scute) of desert tortoise shells consists of incrementally grown laminae in which various bioaccumulated trace elements are sequestered during scute deposition. Laser ablation ICP-MS examination of laminae in scutes of dead tortoises revealed patterns of trace elemental distribution from which the chronology of elemental uptake can be inferred. These patterns may be of pathologic significance in the case of elemental toxicants such as arsenic, which has been linked to both shell and respiratory diseases. Laser ablation transects, performed along the lateral surfaces of sectioned scutes, offered the most successful means of avoiding exogenous contamination that was present on the scute exterior. Semiquantitative determination of elemental concentrations was achieved using sulfur, a keratin matrix element, as an internal standard. The results presented here highlight the potential of laser ablation ICP-MS as a diagnostic tool for investigating toxic element uptake as it pertains to tortoise morbidity and mortality.
Published by Elsevier B.V.

Keywords: Laser ablation; ICP-MS; Desert tortoise; Trace elements; Zinc; Arsenic

1. Introduction

The chronology of trace element accumulation in biological samples may provide insight into the relationship between certain species and their surroundings. Patterns of elemental uptake are often reflected in the elemental composition of incrementally grown biological structures such as teeth, mollusk shells, and fish otoliths (Outridge et al., 1995). Biological structures of this type contain discernible physical attributes such as growth laminae or concentric growth rings that are deposited with seasonal or more frequent periodicity. Elemental analytical data having spatial correspondence to these

* Corresponding author. Tel.: +1 760 939 1608/1600; fax: +1 760 939 1617.
E-mail address: michael.seltzer@navy.mil (M.D. Seltzer).

0048-9697/$ - see front matter. Published by Elsevier B.V.
doi:10.1016/j.scitotenv.2004.07.027

features, and the time line implicit therein, may be amenable to meaningful interpretation. Data of this dimension can provide indirect evidence of climatological variation, or reveal extraordinary temporal changes in elemental uptake possibly associated with anthropogenic perturbation of the environment.

An interesting, and previously untested specimen for this type of analytical approach is the shell tissue of the desert tortoise (*Gopherus agassizii*). Desert tortoise shells are composed of bone, and an incrementally grown covering of keratinized tissue (scutes) that can function as a repository for certain bioaccumulated trace elements. Since hard keratinized tissues of this type are virtually isolated from other metabolic activity, resident elemental species have limited mobility (Takagi et al., 1988). It is reasonable to assume therefore, that the incrementally grown scute tissues of the desert tortoise represent a relatively stable, chronological archive of elemental uptake.

Desert tortoise populations in various regions of the southwestern United States have declined in recent decades, resulting in federal designation as a threatened species (Fish and Wildlife Service, 1990). Desert tortoise morbidity and mortality have been attributed to several factors including upper respiratory tract disease (mycoplasmosis) and cutaneous dyskeratosis, a disease state typified by shell lesions (Jacobson et al., 1994; Homer et al., 1998; Christopher et al., 2003). The causes of shell disease are not known, but nutritional deficiencies and environmental toxicosis affect keratinized tissues in other vertebrates (Berry et al., 1997). Elevated levels of various elemental toxicants, arsenic in particular, have been detected in the tissues of desert tortoises exhibiting clinical signs of cutaneous dyskeratosis (Jacobson et al., 1994; Homer et al., 1998; Berry et al., 2001).

Instrumental neutron activation analysis (INAA) has been used to study the trace elemental systematics of tortoise shell scute and bone for toxicological purposes (Knight et al., 1998; Haxel et al., 2000). INAA measurements revealed modest enrichment of some elements in the shells of healthy tortoises, relative to the average composition of the upper continental crust (Taylor and McLennan, 1985). Strong enrichment by certain elements and anomalous variation in elemental ratios were detected in scute from the shells of diseased tortoises. The INAA method, although extremely sensitive, is not otherwise appropriate for direct examination of localized elemental distribution among incrementally grown biological structures, such as would be required to investigate the chronology of elemental uptake. A more effective approach is likely to be one in which the necessary spatial resolution is achieved directly through various microanalytical techniques. X-ray absorption near-edge structure (XANES) techniques have been adapted to permit spatially resolved measurements in biological samples using source beams having cross sections as small as 50 μm. This relatively elaborate technique, which utilizes synchrotron-generated X-ray radiation, was used successfully to examine the distribution and coordination of elemental species in bone and shell fragments from aquatic turtles (Hunter et al., 1997).

Laser ablation inductively coupled plasma mass spectrometry (laser ablation ICP-MS) is a powerful analytical tool that combines sensitive detection of isotopically resolved elemental species with the versatile solid sampling capability of the laser microprobe (Gunther et al., 2000; Russo et al., 2002). Laser ablation ICP-MS represents an attractive alternative to the XANES approach. The ability to focus the laser beam to a small spot size permits direct sampling of individual microscopic features on a sample surface. When operated in a scanning mode, laser ablation permits ICP-MS measurement of micro-spatial variations in elemental composition along selected transect axes.

There are numerous examples in which laser ablation ICP-MS has been used to analyze elemental distribution in growth bands, laminae, and rings present in various hard biological tissues (Outridge et al., 1995). Analyses of teeth from humans, rodents, and marine mammals have revealed interesting elemental distributions with conspicuous chronological patterns (Evans and Outridge, 1994; Evans et al., 1995; Cox et al., 1996; Lee et al., 1999; Lochner et al., 1999; Ghazi et al., 2000). Laser ablation ICP-MS examination of reef corals has yielded elemental ratios that were highly correlated to sea surface temperature (McCulloch et al., 1999). Accumulated vanadium concentrations in corals, detected during similar studies, were attributable to specific incidents of marine oil pollution (Guzman and Jarvis, 1996). Data obtained during laser ablation ICP-MS measurement

of several metals in mollusk shells exhibited distinct cyclic variations having annual periodicity and reasonable correlation with seasonal fluctuations in algal biomass, seawater chemistry, and temperature (Perkins et al., 1991; Pearce et al., 1992; Imai, 1992; Fuge et al., 1993; Raith et al., 1996; Vander Putten et al., 2000). Laser ablation ICP-MS analyses of fish otoliths, used for elemental fingerprinting to identify various stocks, have also revealed spatial and temporal differences in metal concentration that reflect variations in water chemistry (Campana et al., 1994; Thorrold and Shuttleworth, 2000). Laser ablation ICP-MS examination of trace element concentrations in tissues dissected from banded water snakes (Jackson et al., 2003) further illustrates the potential of this technique for ecotoxicological studies.

Our objective was to assess the utility of laser ablation ICP-MS techniques for measuring differences in elemental content among successive growth laminae of scutes on desert tortoise shells. The relatively thin layer of scute tissue consists of cornified β-keratin containing 10.9% cysteine (Homer et al., 2001) and a corresponding abundance of sulfhydryl bonds. During scute development, various trace elements are sequestered in scute tissue as a result of strong complexation with the sulfhydryl bonds. Scutes are similar to human nails (Takagi, 1988; Rodushkin and Axelsson, 2000) in this respect, and are likely to be of comparable investigative value. The growth rings, as they appear on the surface of the scutes, represent the concentric margins of incrementally grown laminae. It was previously assumed that only one growth ring was formed yearly in most species of turtles (Germano and Bury, 1998). In the desert tortoise, estimating approximate age by counting growth rings is complicated. Juvenile tortoises produce variable numbers of rings in different years, and no rings in drought years (Berry, 2002; Wilson et al., 2003). So-called "false rings" or "accessory lines" have been attributed to periods of slower growth within a given year and are difficult to distinguish from those associated with new layers of keratin (Wilson et al., 2003). Older laminae, including the neonatal areola region, are gradually worn away over time, and only the most recently grown laminae may be available for analytical examination.

To achieve our objective, we first needed to determine if exogenous contamination occurs on the scutes, and if so, design a method to avoid it. Surface and subsurface exogenous contamination has been observed during laser ablation ICP-MS examination of trace elements in human nails (Rodushkin and Axelsson, 2003). The desert tortoise, being a terrestrial burrowing animal, is in almost perpetual contact with soil, and consequently, residual amounts of various mineral elements are likely to be present on the surface of its shell. Exogenous contamination poses a significant challenge since it is difficult, if not impossible to distinguish between elemental species adhering to (or imbedded in) the scute surface, and elemental species chemically sequestered within the keratin matrix as a result of bioaccumulation. The laser ablation ICP-MS and sample preparation methods described below have enabled direct examination of the elemental composition of the scute interior while avoiding exogenous contamination on the scute exterior.

2. Material and methods

2.1. Instrumentation

The present investigation was conducted using a PQ ExCell ICP-MS instrument (Thermo Elemental, Franklin, MA). A UP266 laser ablation accessory (New Wave/Merchantek, Fremont, CA) was operated in a highly integrated manner with the ICP-MS instrument through a software patch. The laser ablation accessory was equipped with an autofocus feature that helped ensure a constant laser spot size and energy density on the sample surface. A 1.0 l/min flow of helium carrier gas was used to entrain sample aerosols from the ablation cell to the plasma torch. A 0.80-l/min stream of argon was combined with the carrier gas at a location close to the base of the plasma torch, to enhance plasma sample introduction. Additional ICP-MS and laser ablation operating conditions are given in Table 1.

2.2. Tortoise shell specimens, exogenous contamination, scute anatomy, and sample preparation

Scutes used as test specimens during laser ablation ICP-MS methods development were obtained from a series of collected shell remains. Scute samples, on

Table 1
LA-ICP-MS instrument operating parameters

Plasma	
Plasma coolant gas (argon)	13.0 l/min
Auxiliary gas (argon)	1.1 l/min
Sample introduction gas (argon)	0.80 l/min
Plasma RF power	1350 W
Ion optics	
Extraction	−600 V
Lens 1	+3.2 V
Lens 2	−69.0 V
Lens 3	−181 V
Deflector	−30.0 V
Focus	+21.6 V
Pole bias	−1.0 V
Data acquisition (TRA)	
Dwell time	50 ms
TRA duration	variable
Scanning mode	peak hopping
Channels per mass	1
Dead time correction	35 ns
Laser ablation	
Laser wavelength	266 nm
Laser pulse duration	4–6 ns
Laser spot size	100 μm
Laser energy at 266 nm	~1.1 mJ/pulse
Repetition rate	20 Hz
Transect rate	100 μm/s
Carrier gas flow (helium)	1.0 l/min

which subsequent analytical measurements were performed, were obtained from the preserved remains of 18 diseased or injured tortoises previously salvaged for necropsy (Homer et al., 1998). The necropsied tortoises included controls (healthy individuals) and tortoises with several diseases. Conventional ICP-MS elemental analysis of parts or entire scutes was undertaken post-necropsy for those specimens (Berry et al., unpublished data, U.S. Geological Survey). Table 2 lists information relevant to the representative set of necropsied tortoise specimens for which we report analytical results.

Laser ablation samples consisted of scutes corresponding to vertebral, costal, and marginal locations (Zangerl, 1969) on the posterior region of the shell carapace. The growth rings on some of these scutes are often less-worn and more distinct in appearance than those observed elsewhere on the shell, and are customarily used for age estimation (Berry, 2002). The specimens examined included disarticulated scutes, and individual scutes that required separation from the underlying bone of intact tortoise shells. Fig. 1 is a photograph of a costal scute on which the areola or "hatchling plate", and growth rings that delineate the incrementally grown laminae, can be seen. The scute structure lends itself to microanalysis interrogation aimed at associating localized trace element concentrations with the chronological sequence in which the laminae were deposited. Examination of elemental distribution, corresponding to a period of time between tortoise hatching and death as a juvenile or young adult, was made possible by the fortuitous presence of areolae and adjoining laminae on most of the specimens.

During laser ablation methods development, it was determined that exogenous contamination on the dorsal scute exterior was likely to obscure patterns of endogenous elemental distribution associated with metabolic uptake of trace elements. Various attempts at cleaning the scute exterior proved ineffective for removing all but superficial amounts of exogenous contamination. These observations prompted us to examine the feasibility of performing laser ablation transects along the lateral surfaces of scute sections. It

Table 2
Tortoise specimens

ID[a]	Sex	MCL[b] (mm)	Weight (kg)	Estimated age	Condition	Disease state	Keratin sulfur concentration[d] (ppm)
#27	M	178	0.90	Adult	Alive—salvaged for necropsy	Healthy tortoise	14,000
#19	F	252	2.3	Adult	Alive—salvaged for necropsy	Mycoplasmosis	15,700
#31	M	271	3.73	Adult	Alive—salvaged for necropsy	Inflammation[c]	15,400
#32	F	210	1.75	Adult	Alive—salvaged for necropsy	Cutaneous dyskeratosis	15,700

[a] Descriptions from Homer et al. (1998).
[b] Midline carapace length.
[c] Inflammation of chin glands, nasal cavity, eyelids and salivary glands.
[d] Berry et al. (unpublished data), U.S. Geological Survey.

Fig. 1. Photograph of a costal scute showing the areola and successive growth rings.

was presumed that sampling the exposed interior regions of the scutes would enable access to incrementally grown structures while largely avoiding the effects of exogenous contamination.

Although growth rings are easily discernible on the external surface of the scute, the histology of the scute interior is not obvious. The mechanism by which new scute tissue is deposited is also not well understood. It has been speculated that as the epidermis grows, the outer cells die and harden, forming a layer of scute (Wilson et al., 2003). Following cessation of growth, a new layer of scute is formed underneath an existing layer, and most evidently, along its periphery. The hypothetical arrangement of laminae depicted in Fig. 2 is consistent with the gradual decrease in scute thickness observed between the areola and the distal edge of scutes, and also, the retention of a thin layer of scute tissue following the wearing away of older laminae from desert tortoises. Fig. 2 also illustrates the approximate orientation of a laser ablation transect axis along the lateral surface of the scute section.

Prior to sectioning, a plastic brush and deionized water were used to remove soil and other debris from scute samples. Scute sections, 2–3 mm in width, were cut along axes orthogonal to the visible growth rings using a 0.48-mm-thick alumina-coated wafering saw. Warm acetone was used to remove residues of mounting wax used during the sectioning procedure. Individual scute sections were affixed to glass slides for laser ablation experiments using double-sided adhesive tape.

2.3. Laser ablation and data acquisition

Laser ablation transects were performed along the lateral surfaces of sectioned scutes to examine the intrinsic elemental composition of the scute interior. Transects were initiated at a location on the exposed lateral surface coincident with the areola, or otherwise oldest tissue. The transects proceeded towards the distal end of each scute specimen, in a direction orthogonal to the growth rings visible on the scute exterior. Based on the nominal transect rate, it was possible to associate recorded ion intensities with specific distances along the transect axes, and thereby construct transect profiles of elemental concentration. Ablation patterns followed the general contour of the scute section (Fig. 2) but were offset approximately 100 μm from the external surface to avoid imbedded contaminants.

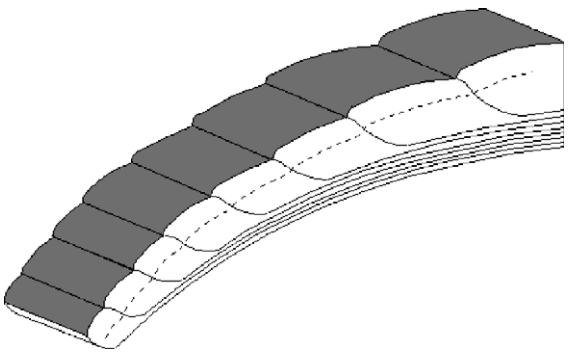

Fig. 2. Notional diagram of sectioned scute specimen illustrating a supposed arrangement of incrementally grown laminae. The laser ablation transect axis is represented by a dotted line.

Laser ablation patterns consisted of a line of overlapping 100-μm diameter craters. A laser repetition rate of 20 Hz was used along with a transect rate of 100 μm/s. Clean-up scans were performed on each scute sample to remove contaminants that may have been re-distributed from the scute exterior during the sectioning procedure. Multiple analytical scans were then performed over the same transect axis to examine data reproducibility, and allow identification of spurious responses arising from re-condensation of ablated material.

During laser ablation transects on scute samples, the ion intensities of $^{33}S^+$, $^{51}V^+$, $^{55}Mn^+$, $^{59}Co^+$, $^{65}Cu^+$, $^{66}Zn^+$, $^{75}As^+$, $^{111}Cd^+$, and $^{208}Pb^+$ were acquired in the time resolved analysis (TRA) mode. TRA "time slices" corresponded to successive 50-ms dwell intervals for each atomic mass. The 50-ms dwell intervals represented a compromise between maximizing the number of sweeps of the atomic mass range per unit time, and moderating the size of the collected data file in each instance. Dwell intervals of shorter duration did not appear to enhance the fidelity of the resulting transect profiles. Correction for the $^{40}Ar^{35}Cl^+$ polyatomic interference on $^{75}As^+$ was performed automatically, and amounted to no more than a few hundred counts in each instance.

2.4. Measurement of elemental concentrations

A principal deficiency of laser ablation-based spectroanalytical techniques is the lack of suitable matrix-matched calibration standards. Semiquantitative analysis schemes, based on available internal standard elements, represent a functional alternative for samples that contain a reasonably homogeneous matrix (Van de Weijer et al., 1992; Craig et al., 2000). Tortoise shell scute is a viable candidate for this approach. Sulfur, which is uniformly concentrated in scute keratin at approximately 1.5 wt.% in adult desert tortoises, was selected as an internal standard for the present investigation. While not an ideal internal standard for reasons outlined below, sulfur was the only practical choice in this instance. For the purposes of this application, we postulated that the measured ion intensities of sulfur and various trace element isotopes could be used in conjunction with the percent abundance of each isotope, and the generalized response curve of the ICP-MS instrument, to estimate the concentrations of individual trace elements in the scute sample. The composite sulfur concentrations of scute samples from individual tortoise specimens, determined using independent elemental analysis, are listed in Table 2.

Plasma conditions under the present instrument configuration are considerably different from those encountered during conventional aqueous sample introduction. The dry plasma associated with laser ablation, and the addition of helium as a sample carrier gas, are likely to affect analyte residence times and ionization yields to the extent that the relative sensitivity factors (RSFs) used during aqueous sample introduction, are no longer valid. The selection of sulfur as an internal standard further complicates the situation. Sulfur lies near the lower end of the atomic mass range and also is poorly ionized relative to most transition metals. It was therefore necessary to perform experiments to estimate interelement sensitivity factors, appropriate to these conditions, to enable semiquantitative determination of elemental concentrations.

The standard reference material (SRM), NIST 1566b Oyster Tissue, contains certified concentrations of sulfur and various trace elements as well as noncertified amounts of other elements (Table 3). The sulfur content of the SRM is 0.6887 ± 0.0140 wt.% (6887 ± 140 ppm), slightly less than one-half that contained in tortoise scute. Homogeneous mixtures containing 0.45 g of the powdered oyster tissue and 0.05 g of paraffin binder (Spex CertiPrep, Metuchen, NJ) were introduced into a 13-mm pellet die. Sample pellets were prepared by subjecting the mixtures to an applied load of 10 metric tons. Ion optics and gas flow settings (Table 1) were optimized while monitoring the $^{111}Cd^+$ ion intensity during ablation of the SRM pellet. Following optimization, five replicate ablation scans were performed on the SRM pellet using conditions identical to those used for ablation scans on scute samples. The ion intensities of $^{33}S^+$, $^{51}V^+$, $^{55}Mn^+$, $^{57}Fe^+$, $^{59}Co^+$, $^{65}Cu^+$, $^{70}Zn^+$, $^{75}As^+$, $^{85}Rb^+$, $^{88}Sr^+$, $^{107}Ag^+$, $^{111}Cd^+$, and $^{208}Pb^+$ were recorded. Gas blanks were subtracted in each instance to obtain net ion intensities. A series of interelement sensitivity factors were then calculated based on the average ion intensities, the isotopic abundance of the associated ions, and certified concentrations of the corresponding elements. It is

Table 3
Interelement sensitivity factors

Element	Isotope	Percent isotopic abundance	Average ion intensity (cps)	Certified concentration[a] (ppm)	Sensitivity (cps/ppm)[b]	Interelement sensitivity factor
Sulfur	^{33}S	0.75	330445	6887±140	6397	1.00
Vanadium	^{51}V	99.5	57407	0.577±0.023	99732	15.6
Manganese	^{55}Mn	100	2781640	18.5±0.2	150359	23.5
Iron	^{57}Fe	2.2	571454	205.8±6.8	123411	19.3
Cobalt	^{59}Co	100	44906	0.371±0.009	121041	18.9
Copper	^{65}Cu	30.83	2319489	71.6±1.6	105077	16.4
Zinc	^{70}Zn	0.62	782931	1424±46	88679	13.9
Arsenic	^{75}As	100	128946	7.65±0.65	16856	2.63
Rubidium	^{85}Rb	72.165	430948	3.262±0.145	183219	28.6
Strontium	^{88}Sr	82.58	953808	(6.8±0.2)[c]	169896	26.6
Silver	^{107}Ag	51.35	58804	0.666±0.009	171945	26.9
Cadmium	^{111}Cd	12.8	37750	2.48±0.08	118365	18.5
Lead	^{208}Pb	52.4	43682	0.308±0.009	270658	42.3

[a] NIST SRM 1566b oyster tissue.
[b] Normalized to isotopic abundance.
[c] Value in parentheses represents a noncertified trace element concentration.

worth noting that the high concentration of zinc in the SRM necessitated the use of the low-abundance ^{70}Zn isotope (0.62% abundance). The more moderate concentrations of zinc encountered in scute keratin can be quantified using the ^{66}Zn (27.81% abundance) or ^{67}Zn (4.11% abundance) isotopes.

3. Results

3.1. Interelement sensitivity factors

Table 3 lists the average ion intensities, percent abundances, certified concentrations, and interelement sensitivity factors calculated for each of the elements in the SRM. All values are referenced to the sulfur internal standard. The following expression was derived to enable semiquantitative determination of trace element concentrations in scute based on relative ion intensities measured for $^{33}S^{+}$ and concomitant analytes, and incorporating the interelement sensitivity factors listed in Table 3:

$$[\mathrm{M}] = \frac{I(^{x}\mathrm{M}^{+})}{I(^{33}\mathrm{S}^{+})} \times \frac{F_{(\mathrm{S})}A(^{33}\mathrm{S})}{F_{(\mathrm{M})}A(^{x}\mathrm{M})} \times [\mathrm{S}]$$

where: [M]=trace element analyte concentration (ppm); $I(^{x}M^{+})$=ion intensity of trace element isotope; $I(^{33}S^{+})$=ion intensity of sulfur isotope; $F_{(S)}$=relative sensitivity factor for sulfur=1.00; $F_{(M)}$=relative sensitivity factor for trace element analyte; $A(^{33}S)$=percent abundance for sulfur isotope; $A(^{x}M)$=percent abundance for trace element isotope; [S]=sulfur concentration (ppm).

The interelement sensitivity factors listed in Table 3 reflect differences in both sample introduction and instrumental response, between the sulfur internal standard and various analyte elements in the SRM, which served in the present case as a surrogate for tortoise scute. Because it cannot be assumed that sample matrix effects such as elemental fractionation (Chen, 1999) are similar in scute, it is understood that elemental concentrations determined on the basis of these factors, are strictly semiquantitative.

3.2. Laser ablation transects

Laser ablation transects were intended to reveal localized elemental concentrations in the scute tissue and patterns of elemental sequestration among successive laminae. Following acquisition of analyte ion intensities, elemental concentrations were calculated, based on the semiquantitative scheme described in Section 2.4. A series of plots (transect profiles) illustrating elemental distribution along the transect axis were then generated. Data smoothing was

performed in each instance to discriminate against spurious signals, and to highlight significant features in the transect profiles. The transect profile data presented below illustrate the capability of the laser ablation ICP-MS technique for examining differences in elemental distribution between shell tissues of both healthy and diseased tortoises.

Fig. 3A includes transect profiles showing the distribution of zinc along the lateral surface of a sectioned scute specimen obtained from tortoise #27. Repetitive ablation scans over the same transect axis revealed nearly identical patterns of zinc concentration. Fig. 3B shows the distribution of arsenic along the same transect as that corresponding to the zinc data in Fig. 3A. Concentration patterns of other trace elements in this sample were unremarkable. Figs. 4A, 5A and 6A represent transect profiles of zinc concentration associated with specimens #19, #31, and #32, respectively. Each of these transect profiles, along with that shown in Fig. 3A consist of a series of concentration maxima of varying amplitude. In several instances, concentration maxima exhibited unresolved shoulders that likely correspond to the accessory rings or lamina substructures described earlier. It is interesting to note that the number of concentration maxima observed in each transect profile is approximately equal to the number of growth rings discernible on the exterior of the corresponding scutes.

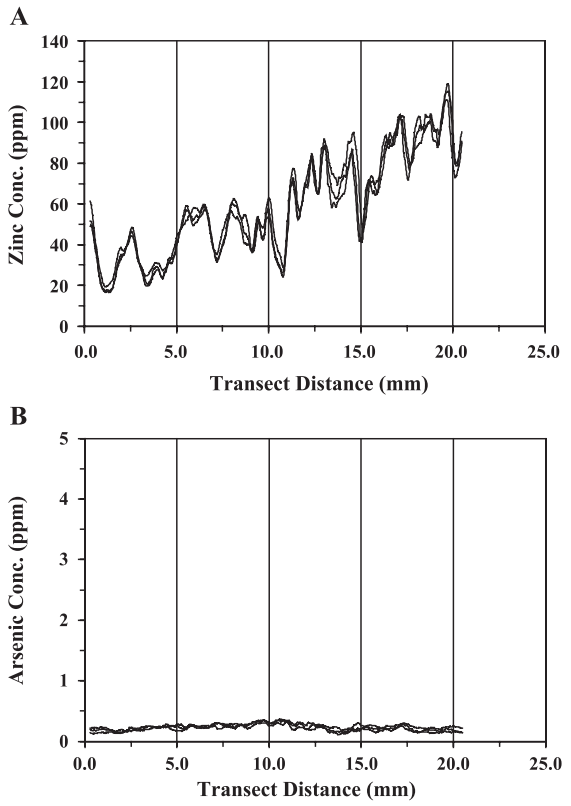

Fig. 3. Transect profiles of zinc (A) and arsenic (B) representing three consecutive ablation scans on scute section from tortoise specimen #27 (control sample).

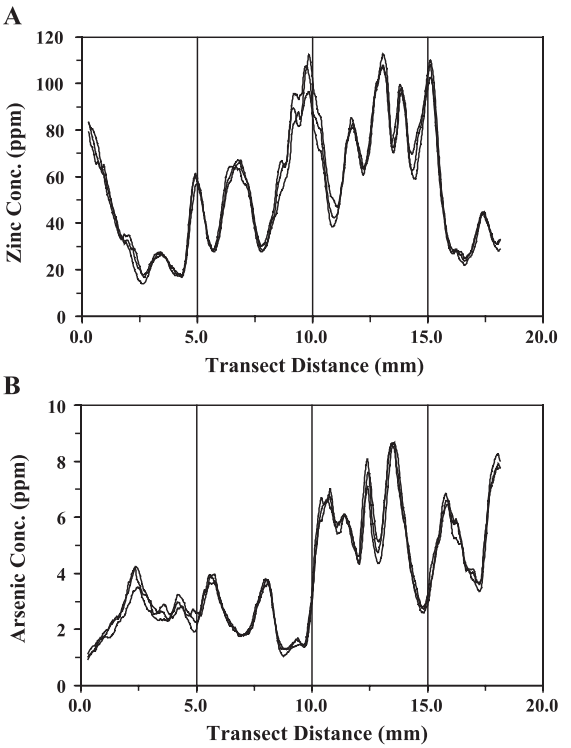

Fig. 4. Transect profiles of zinc (A) and arsenic (B) representing three consecutive ablation scans on scute section from tortoise specimen #19 (diseased tortoise).

While the patterns of zinc concentration shown in Figs. 4A, 5A and 6A are generally similar in appearance to that shown in Fig. 3A, the patterns of arsenic concentration associated with these specimens exhibit some notable differences. Arsenic concentrations are elevated throughout the transect profile depicted in Fig. 4B, and appear to increase late in the transect. Arsenic concentrations near the beginning of the transect shown in Fig. 5B are comparable to the baseline levels depicted throughout Fig. 3B, but

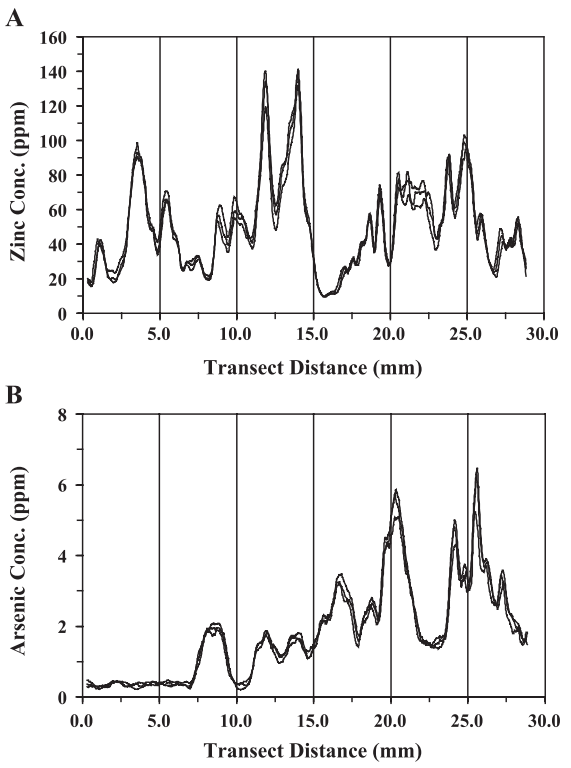

Fig. 5. Transect profiles of zinc (A) and arsenic (B) representing three consecutive ablation scans on scute section from tortoise specimen #31 (diseased tortoise).

increase in magnitude thereafter. The transect profile in Fig. 6B shows a series of minor concentration maxima near the beginning of the transect, and reveals highly elevated concentrations of arsenic in the latter half of the transect, near or after the time the tortoise reached adult size. Net concentrations, and concentration patterns for elements other than zinc and arsenic in scutes from tortoises #19, #31, and #32 were unremarkable.

Survey ablation transects, performed on the dorsal exterior surfaces of scute specimens #19, #27, #31, and #32, confirmed the presence of exogenous zinc contamination. Exogenous arsenic contamination was clearly evident on scute specimen #32, and to a lesser extent on #31 and #19. Exogenous arsenic contamination was conspicuously absent from the dorsal surface of scute specimen #27. The contribution of exogenous contamination to the elemental content of bulk scute samples is discussed in Section 4.3.

3.3. Comparison of results from laser ablation ICP-MS with post-necropsy analyses

Although the laser ablation ICP-MS technique was used specifically to reveal localized elemental concentrations along a given transect axis, it was possible to estimate average elemental concentrations in scute samples using transect profile data. We compared these results with those obtained through analyses of scutes from tortoises #19, #27, #31, and #32 at the time of necropsy (Berry et al., unpublished data, U.S. Geological Survey). Different scutes from each tortoise were used for laser ablation ICP-MS, and for conventional ICP-MS analyses. In addition, chemical digestion of parts or whole scutes enables recovery of analytes in a manner that more accurately reflects the macroscopic composition of the scutes.

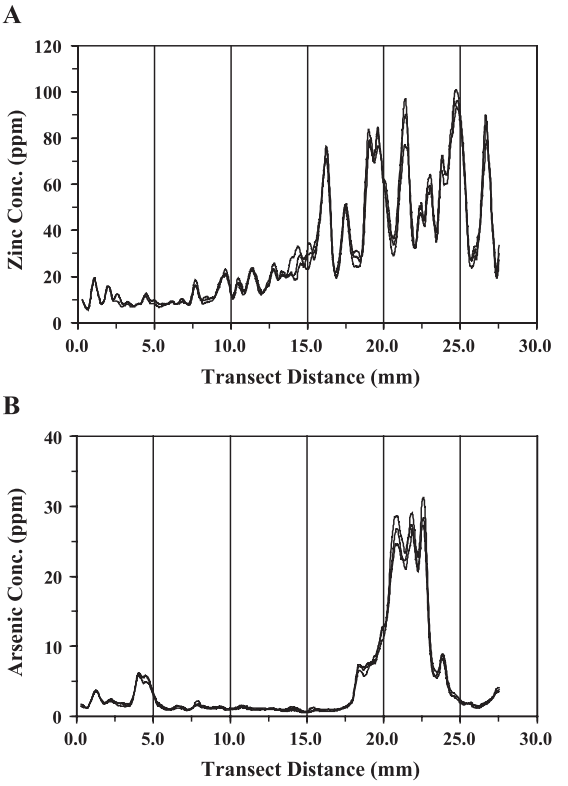

Fig. 6. Transect profiles of zinc (A) and arsenic (B) representing three consecutive ablation scans on scute section from tortoise specimen #32 (diseased tortoise).

Table 4
Comparison between laser ablation ICP-MS results and post-necropsy analyses of scute samples

Tortoise specimen	Zinc concentration		Arsenic concentration	
	Laser ablation ICP-MS[a] (ppm)	Conventional ICP-MS[b] (post-necropsy) (ppm)	Laser ablation ICP-MS[a] (ppm)	Conventional ICP-MS[b] (post-necropsy) (ppm)
#27	59.9	51	0.2	<2
#19	51.3	37	3.6	11
#31	46.4	44	1.4	<2
#32	30.6	28	5.3	15

[a] Concentration averaged over laser ablation transect profile.
[b] Composite concentration in bulk scute sample; Berry et al. (unpublished data), U.S. Geological Survey.

Table 4 lists concentrations of zinc and arsenic, averaged over laser ablation transect profiles, along with post-necropsy values for each of the four specimens. Agreement between zinc concentrations in all four specimens is reasonable, while significant discrepancies are evident for the arsenic results. The concentrations of arsenic in scutes from tortoises #19 and #32 in particular, are lower than the corresponding post-necropsy values by a factor of 3. Although these scutes were first cleaned and rinsed, it is possible that measurement discrepancies noted above are attributable to the net contribution of exogenous contamination to the total amount of arsenic recovered during chemical digestion of the samples.

4. Discussion

4.1. Interpretation of results—patterns of zinc concentration

Figs. 3–6 illustrate patterns of zinc concentration obtained by performing laser ablation transects in a direction orthogonal to the principal growth axis of each scute segment. Nearly identical patterns were observed following repeated transects, during which successive amounts of material were sampled from the scute interior. The consistency of these patterns substantiates the notion that the zinc concentrations represented are entirely endogenous in nature. Slight variations among the repetitive scans are probably indicative of microscale elemental heterogeneity in the scute samples. These results suggest that laser ablation transects, performed along the lateral surfaces of section scutes, achieved a level of spatial resolution and structural differentiation comparable to that expected for laser ablation transects performed on the scute exterior. Furthermore, the successful acquisition of distinct concentration patterns, especially those depicting zinc distribution, lend certain credibility to the hypothetical arrangement of scute laminae illustrated in Fig. 2. Patterns of zinc concentration may be useful as a map of the scute interior as well as a spatial reference for the distribution of other trace elements.

4.2. Interpretation of results—patterns of arsenic concentration

Patterns of arsenic concentration in the scute tissues of diseased tortoises and their associated chronologies may be particularly informative. Tortoise #27 was used as a control specimen for the present investigation since it was determined via necropsy examination to be a healthy tortoise (Homer et al., 1998). The laser ablation transect profile shown in Fig. 3B indicates arsenic concentrations below 1 ppm. The general absence of arsenic in this scute is consistent with the results of post-necropsy elemental analyses of scute from the same tortoise (Table 4), and is typical of the majority of examined specimens. Laser ablation ICP-MS examination of three other necropsied specimens (#19, #31, and #32) revealed patterns of elevated arsenic concentration. For tortoise #19, arsenic was elevated in the scute throughout the transect (Fig. 4B), including the early portion associated with the neonatal areola tissue. A series of concentration maxima observed later in the transect are indicative of arsenic uptake in subsequent years, probably at or near the time of adulthood. In tortoise #31, arsenic concentration is not elevated in the early portion of the transect, and only moderately elevated thereafter. For tortoise #32, arsenic levels were

moderately elevated at certain locations early in the transect and highly elevated over a sustained region in the latter part of the transect. Arsenic concentration in #32 subsequently diminished to baseline levels indicating possible cessation in uptake of this element.

It is significant that all three tortoises having elevated arsenic levels were ill, #19 with mycoplasmosis, #31 exhibiting inflammation of chin glands, nasal cavity, eyelids and salivary glands, and #32 with cutaneous dyskeratosis and necrotizing epidermitis (Homer et al., 1998). Elevated arsenic levels have been found in scutes, livers, and kidneys of necropsied tortoises ill with mycoplasmosis, cutaneous dyskeratosis, and other diseases compared with control or healthy tortoises (Berry et al., 2001). However, correlative studies using necropsied tortoises are preliminary in nature, and are a small part of a much larger research program on diseases in desert tortoises. Arsenic and other elemental toxicants have been demonstrated to deleteriously affect the well-being of domestic and wild animals (Blood and Radostits, 1989). Although not confirmed through systematic investigation, arsenic intoxication appears to be one of several causative factors in tortoise morbidity and mortality.

Arsenic and other elemental toxicants are naturally abundant in the desert environment. However, the environments that tortoises live in now are different than those occupied 100–150 years ago. In certain areas of the desert, mining operations, disturbances of playa surfaces, and other human-related activities, have resulted in remobilization and concentration of elemental toxicants in the air, on the soil surface, and on the surfaces of forage plants (Chaffee and Berry, in press). The inhalation of dust and ingestion of contaminated vegetation and soil particles by tortoises in those areas are probable pathways for arsenic intake.

The patterns of zinc and arsenic concentration revealed using laser ablation ICP-MS, in the scute samples described above, illustrate the potential of this microanalytical technique for examining elemental distribution in incrementally grown biological structures. Patterns of zinc, an essential nutrient, appear to closely mirror the incremental deposition of scute tissue. However, the corresponding arsenic patterns illustrated in Figs. 4–6 exhibit only limited spatial correlation with those of zinc. Reduced or discontinuous uptake of arsenic during periods of time of no or little growth of lamina (Figs. 4 and 5), and sustained uptake of arsenic over multiple growth periods (Fig. 6), are plausible explanations for this phenomenon.

4.3. Interpretation of results—potential effects of exogenous contamination on scute analyses

The detection of exogenous contaminants on the dorsal surfaces of certain scutes demonstrates the inefficacy of common cleaning methods for removal of these species prior to analyses. A systematic examination of washing techniques used prior to ICP-MS, and laser ablation ICP-MS analyses of human nails revealed considerable disparity in the degree to which various exogenous elements are removed from sample surfaces, and the significant potential for measurement bias under these circumstances (Rodushkin and Axelsson, 2000, 2003). Similarly, the inadvertent inclusion of residual surface contaminants among analytes recovered from chemically digested scutes may be an impediment to the meaningful determination of endogenous trace elements in the bulk of the scute.

Discrepancies between the average concentrations of arsenic derived from transect profile data and those obtained during post-necropsy analyses of scutes from the same specimens can be rationalized in view of the fundamental experimental differences cited above. However, the influence of exogenous arsenic contamination on the latter results may also be significant. In this respect, laser ablation ICP-MS, as performed in the present instance, appears to offer certain advantages for differentiating between exogenous and endogenous elemental concentrations. Discrepancies between zinc values from the two analytical methods were less pronounced, despite the presence of exogenous zinc contamination on all three scute specimens. It is very likely that the total amount of zinc recovered during post-necropsy analyses was dominated by the endogenous component.

Although further refinement and validation of the semiquantitative measurement scheme is warranted, the results presented here indicate that this approach is adequate, absent a quantitative analysis scheme based on matrix-matched calibration standards. Efforts to optimize detection sensitivity and additional contamination control procedures will be required to permit examination of trace elements having concentrations

in scute tissues lower than those encountered during the present investigation.

5. Conclusions

We have successfully demonstrated the use of laser ablation ICP-MS techniques for examining trace element distribution in the incrementally grown laminae of scute tissues from the shells of dead desert tortoises. Laser ablation transects performed along the lateral surfaces of sectioned scutes offered the most successful means of avoiding exogenous contamination that was present on the scute exterior. Transect profiles of trace element concentration obtained in this manner revealed patterns that, in all probability, reflect the actual chronology of elemental uptake. Laser ablation ICP-MS detection of localized, elevated concentrations of arsenic in the scute tissues obtained from diseased tortoises may provide a useful indication of the approximate age at which the corresponding arsenic uptake occurred. These findings are of pathologic significance, given the suspected role of arsenic and other elemental toxicants in desert tortoise morbidity and mortality. We anticipate that the investigative capability demonstrated here could also be useful for analyzing shell-skeletal remains of tortoises from various regions of the desert as part of epidemiological surveys.

Acknowledgments

Funding was provided by the Naval Air Weapons Station Range Environmental Department, the U.S. Geological Survey, and the Bureau of Land Management (necropsies). Scientific research permits for necropsies and shell-skeletal remains were issued to K.H. Berry by the U.S. Fish and Wildlife Service and the California Department of Fish and Game. We thank K. Phillips for reviewing the manuscript.

References

Berry KH. Demographic consequences of disease in two desert tortoise populations in California, USA. Proceedings: Conservation, restoration, and management of tortoises and turtles—an international conference, New York Turtle and Tortoise Society, p. 91–9.

Berry KH. Using growth ring counts to age juvenile desert tortoises (*Gopherus agassizii*) in the wild. Chelonian Conserv Biol 2002;4:416–24.

Berry KH, Homer BL, Alley W, Chaffee M, Haxel G. Health and elevated mortality rates in desert tortoise populations: the role of arsenic and other potential toxicants. Arsenic Group Meeting, U.S. Geological Survey, Denver, CO. February 21–22, 2001.

Blood DC, Radostits OM. Veterinary medicine: a textbook of the diseases of cattle, sheep, pigs, goats and horses. 7th edition. London: Baillière Tindall; 1989. 1502 pp.

Campana SE, Fowler AJ, Jones CM. Otolith elemental fingerprinting for stock identification of Atlantic cod (*Gadus morhua*) using laser ablation ICP-MS. Can J Fish Aquat Sci 1994;51:1942–50.

Chaffee MA, Berry KH. Abundance and distribution of selected elements in soils, stream sediments, and selected forage plants from desert tortoise habitats in the Mojave and Colorado Deserts, USA. J Arid Environ [in press].

Chen Z. Inter-element fractionation and correction in laser ablation inductively coupled plasma mass spectrometry. J Anal At Spectrom 1999;14:1823–8.

Christopher MM, Berry KH, Henen BT, Nagy KA. Clinical disease and laboratory abnormalities in free-ranging desert tortoises in California (1990–1995). J Wildl Dis 2003;39(1):35–56.

Cox A, Keenan F, Cooke M, Appleton J. Trace element profiling of dental tissues using laser ablation-inductively coupled plasma mass spectrometry. Fresenius' J Anal Chem 1996;354:254–8.

Craig CA, Jarvis KE, Clarke LJ. An assessment of calibration strategies for the quantitative and semi-quantitative analysis of calcium carbonate matrices by laser ablation-inductively coupled plasma-mass spectrometry (LA-ICP-MS). J Anal At Spectrom 2000;8:1001–8.

Evans RD, Outridge PM. Applications of laser ablation inductively coupled plasma mass spectrometry to the determination of environmental contaminants in calcified biological structures. J Anal At Spectrom 1994;9:985–9.

Evans RD, Richner P, Outridge PM. Micro-spatial variations of heavy metals in the teeth of walrus as determined by laser ablation ICP-MS: the potential for reconstructing a history of metal exposure. Arch Environ Contam Toxicol 1995;28:55–60.

Fish and Wildlife Service. Endangered and threatened wildlife and plants; determination of threatened status for the Mojave population of the desert tortoise. Fed Reg 1990;55(63):12178–91.

Fuge R, Palmer TJ, Pearce NJG, Perkins WT. Minor and trace element chemistry of modern shells: a laser ablation-inductively coupled plasma mass spectrometry study. Appl Geochem 1993;2:111–6.

Germano DJ, Bury RB. Age determination in turtles; evidence of annual deposition of scute rings. Chelonian Conserv Biol 1998;3:123–32.

Ghazi AM, Shuttleworth S, Angula S, Pashley D. Quantitative measurements of gallium diffusion across human root dentin. J Anal At Spectrom 2000;15:1335–41.

Gunther D, Horn I, Hattendorf B. Recent trends and developments in laser ablation ICP-mass spectrometry. Fresenius' J Anal Chem 2000;368:4–14.

Guzman HM, Jarvis KE. Vanadium century record from Caribbean reef corals: a tracer of oil pollution in Panama. Ambio 1996; 25:523–6.

Haxel GB, Knight RJ, Berry KH, Homer BL, Chaffee MA. Trace element systematics of desert tortoise shell. Twenty-Fifth Annual Meeting and Symposium of the Desert Tortoise Council, Las Vegas, NV, April 21–24; 2000.

Homer BL, Berry KH, Brown MB, Ellis G, Jacobson ER. Pathology of diseases in wild desert tortoises from California. J Wildl Dis 1998;34(3):508–23.

Homer BL, Li C, Berry KH, Denslow ND, Jacobson ER, Sawyer RH, Williams JE. Soluble scute proteins of healthy and ill desert tortoises (*Gopherus agassizii*). Am J Vet Res 2001;62:104–10.

Hunter DB, Bertsch PM, Kemner KM, Clark SB. Distribution and chemical speciation of metals and metalloids in biota collected from contaminated environments by spatially resolved XRF, XANES, and EXAFS. J Phys, IV France 1997;7:767–71.

Imai N. Microprobe analysis of geological materials by laser ablation-inductively coupled plasma mass spectrometry. Anal Chim Acta 1992;269:263–8.

Jackson BP, Hopkins WA, Baionno J. Laser ablation ICP-MS analysis of dissected tissue: a conservation-minded approach to assessing contaminant exposure. Environ Sci Technol 2003;37: 2511–5.

Jacobson ER, Wronski TJ, Schumacher J, Reggiardo C, Berry K. Cutaneous dyskeratosis in free-ranging desert tortoises, *Gopherus agassizii*, in the Colorado Desert of Southern California. J Zoo Wildl Med 1994;25:68–81.

Knight RJ, Haxel GB, Berry KH, Wooden JL. Geo–bio-chemistry of the desert tortoise: trace element composition of carapace and scute by neutron activation analysis. Twenty-Third Annual Meeting and Symposium of the Desert Tortoise Council, Vas Vegas, NV, April 3–5; 1998.

Lee KM, Appleton J, Cooke M, Keenan F, Sawicka-Kapusta K. Use of laser ablation inductively coupled plasma mass spectrometry to provide element versus time profiles in teeth. Anal Chim Acta 1999;395:179–85.

Lochner F, Appleton J, Keenan F, Cooke M. Multi-element profiling of deciduous teeth by laser ablation-inductively coupled plasma mass spectrometry. Anal Chim Acta 1999;401:299–306.

McCulloch MT, Tudhope AW, Esat TM, Mortimer GE, Chappell J, Pillans B, Chivas AR, Omura A. Coral record of equatorial sea-surface temperatures during the penultimate deglaciation at Huon peninsula. Science 1999;283:202–4.

Outridge PM, Veinott G, Evans RD. Laser ablation ICP-MS analysis of incremental biological structures: archives of trace-element accumulation. Environ Rev 1995;3:160–70.

Pearce NJG, Perkins WT, Fuge R. Developments in quantitative and semi-quantitative determination of trace-elements in carbonates using laser ablation inductively coupled plasma mass spectrometry. J Anal At Spectrom 1992;7:595–8.

Perkins WT, Fuge R, Pearce NJG. Quantitative analysis of trace elements in carbonates using laser ablation inductively coupled plasma mass spectrometry. J Anal At Spectrom 1991;6:445–9.

Raith A, Perkins WT, Pearce NJG, Jeffries TE. Environmental monitoring of shellfish using UV laser ablation ICP-MS. Fresenius' J Anal Chem 1996;355:789–92.

Rodushkin I, Axelsson MD. Application of double focusing sector field ICP-MS for the multielement characterization of human hair and nails: Part I Analytical methodology. Sci Total Environ 2000;250:83–100.

Rodushkin I, Axelsson MD. Application of double focusing sector field ICP-MS for the multielement characterization of human hair and nails: Part III Direct analysis by laser ablation. Sci Total Environ 2003;305:23–39.

Russo RE, Mao X, Liu H, Gonzalez J, Mao SS. Laser ablation in analytical chemistry—a review. Talanta 2002;57:425–52.

Takagi Y, Matsuda S, Imai S, Ohmori Y, Masuda T, Vinson JA, Mehra MC, Puri BK, Kaniewski A. Survey of trace elements in human nails: an international comparison. Bull Environ Contam Toxicol 1988;41:690–5.

Taylor SR, McLennan SM. The continental crust: its composition and evolution. Oxford (UK): Blackwell Scientific Publications; 1985. 312 pp.

Thorrold SR, Shuttleworth S. In situ analysis of trace elements and isotope ratios in fish otoliths using laser ablation sector field ICP-MS. Can J Fish Aquat Sci 2000;57:1232–42.

Vander Putten E, Dehairs F, Keppens E, Baeyens W. High resolution distribution of trace elements in the calcite shell layer of modern *Mytilus edulis*: environmental and biological controls. Geochim Cosmochim Acta 2000;64:997–1011.

Van de Weijer P, Baeten WLM, Bekkers MHJ, Vullings PJMG. Fast semiquantitative survey analysis by laser ablation inductively coupled plasma mass spectrometry. J Anal At Spectrom 1992; 7:599–603.

Wilson DS, Tracy CR, Tracy CR. Estimating age of turtles from growth rings: a critical evaluation of the technique. Herpetologica 2003;59:178–94.

Zangerl R. The turtle shell, biology of reptilia. In: Gans Carl, editor. Morphology A, vol. 1. New York: Academic Press; 1969. p. 311–39.